Hindawi
Journal of Nanomaterials
Volume 2023, Article ID 8936855, 12 pages
https://doi.org/10.1155/2023/8936855

Research Article

Characterization and Superhydrophobic Anticorrosive Coating of AA-7475/ZrO_2/Polymer Nanocomposites

Anil Kumar Bodukuri,[1] **Aniket Bhanudas Kolekar**,[2] **Rohit Pandey**,[3] **Koli Gajanan Chandrashekhar**,[4] **P. Ram Kumar**,[5] **K. Anandan**,[6] **C. Devanathan**,[7] **Shubhajit Halder**,[8] **and Balkeshwar Singh**[9]

[1]*Department of Mechanical Engineering, Kakatiya University College of Engineering and Technology, Warangal 506009, Telangana, India*
[2]*Department of Mechanical Engineering, Dr. D.Y. Patil Institute of Engineering, Management and Research, Pune 411044, India*
[3]*Department of Mechanical Engineering, Amity University Madhya Pradesh, Maharajpura Dang, Gwalior 474005, MP, India*
[4]*Department of Mechanical Engineering, Sanjeevan Engineering and Technology Institute, Kolhapur 416201, India*
[5]*Department of Chemistry, V.O. Chidambaram College, Tuticorin 628008, India*
[6]*Department of Physics, Academy of Maritime Education and Training (Deemed to be University), Kanathur 603112, India*
[7]*Department of Mechanical Engineering, Rajalakshmi Engineering College, Thandalam, Chennai 602105, India*
[8]*Department of Chemistry, Hislop College, Nagpur 440001, Maharashtra, India*
[9]*Department of Mechanical Design and Manufacturing Engineering, Adama Science and Technology University, Kebele-14, Adama 1888, Ethiopia*

Correspondence should be addressed to Balkeshwar Singh; balkeshwar.singh@astu.edu.et

Received 25 August 2022; Accepted 29 September 2022; Published 10 May 2023

Academic Editor: Ramesh Balasubramanian

An AA-7475 is coated with superhydrophobic (SH) polymer nanocomposites (PNCs), emphasizing the coating's manufacturing, characterization, and anticorrosive qualities. Coating AA-7475 alloy with polyvinyl chloride (PVC), copper stearate (CS), and zirconium oxide (ZrO_2) nanoparticles produces the desired superhydrophobic. Using an X-ray diffractometer, field-emission scanning electron microscopy, Fourier-transform infrared spectrometer, ZrO_2 nanoparticles, CS, and PVC PNCs are analyzed structurally and molecularly. The atomic force microscope picture was analyzed to determine how the surface roughness affected the SH behavior reached by changing the weight percentage of ZrO_2 nanoparticles from 0.6 to 3.0 wt%. PNC-5 with 3.0 wt% ZrO_2 nanoparticles is used as resistance to corrosion coating for AA-7475 due to its water contact angle of 154°. In a 3.5% NaCl solution, uncoated and PNC-5-coated AA-7475 are examined using potentiodynamic polarization and electrochemical spectroscopy. PNC-5 coating reduces AA-7475 corrosion rate from 23.75 to 0.2253 mpy. In this study, we use polarization resistance, corrosion resistance efficiency, double layer capacitance, corrosion current density, and charge transfer resistance to demonstrate that the SH surface air trapping phenomena are responsible for effective corrosion resistance.

1. Introduction

Except for the few noble metals, all other metals oxidize spontaneously in the atmosphere to reach a stable state, making corrosion an inevitable part of their existence [1]. Atmospheric moisture that makes its way to the surfaces of metallic structures promotes the creation of the necessary ions that ultimately lead to the formation of the metal's most stable oxide [2, 3]. Climate change, thermal fluctuation (day and night), environmental pollutants, and corrosive elements like acidic or alkaline compounds all affect the corrosion process [4]. Still, water molecules play the most important role. An oxide layer formed by the spontaneous reaction of aluminum with oxygen and water in the air to produce aluminum oxide can protect the metal against corrosion even in the presence of water [5]. Despite aluminum's inertness in water, its oxide coating quickly deteriorates upon contact with chloride ions [6, 7]. Corrosion of metals occurs when chloride ions penetrate the

oxide layer and catalyze a chemical reaction that forms aluminum chloride and other chemicals [8]. Pits are formed as aluminum chloride dissolves into the water, creating a void that facilitates further corrosion. Alloys of aluminum were used to improve the mechanical and structural qualities [9, 10]. Shipbuilding, coastal equipment, and saltwater desalination are some of the most common applications for the 6xxx Al alloys [11]. For structural applications in the marine industry, AA-7475 alloys are particularly popular. However, aluminum alloys' corrosion resistance is lower than that of pure aluminum [12]. It is necessary to utilize proper coating procedures due to Al-alloy corrosion. Because of its carcinogenic effect on living creatures and high cost, heavy metal chromium should be avoided [13]. Because of this, scientists are searching for more cost-effective and environmentally friendly coating solutions.

Recent years have seen a surge in interest in creating superhydrophobic (SH) coatings among academics. When droplets of water are deposited on SH surfaces, they form a bead-like structure [14, 15]. This is because SH surfaces exhibit assertive water-repellency behavior. A low surface energy material must be deposited onto a substrate with an appropriate roughness to have the SH property [15]. Low surface energy provides hydrophobicity, amplified to a superhydrophobic type by air trapping-induced roughness. Metal corrosion is improved by incorporating a metallic substrate with an SH nature, which does not interact with corroding ions and moisture [16, 17]. Moreover, the air retained on the SH surface prevents the surface from coming into contact with the corrosive chloride ions found in the aqueous medium [18]. Many scientists have worked to build a water-repellent SH coating that can protect metals from corrosion in the chloride-ion-rich maritime atmosphere.

TiO_2 functionalized methyl hydrogen polysiloxane was used by Gao et al. [19] to create SH surfaces on metal by heating the steel first. Corrosion resistance in mild steel is improved by cutting the coating's i_{corr} value from 120.22 to 0.09 A and raising the contact angle with water from 160.7°. To increase the corrosion resistance of the AZ91D alloy, Yin et al. [20] employed thiol-based compounds in a TiO_2/copper/self-assembly approach. To create an SH surface, Yin et al. [21] used a hydrothermal process to coat a dual layer of ZrO_2/SiO_2 over a zinc-based substrate. Using a chemical etching approach, Sharma et al. [22] created SH CuO microneedles to limit the corrosion of copper in the marine atmosphere. By employing the thermal annealing process, Yang et al. [23] produced a water contact angle (WCA)-153° coating with a tilt angle of 5°. Similar to how numerous methods are used in corrosion-resistant manufacturing materials with SH coating, many different approaches have been developed [24]. The methods presented here, however, are not simple enough to be used for SH coating on massive buildings. In addition, the methods used to design SH environments are highly specialized and can only be applied to certain small-scale structures [25]. A nonwettable feature must be imparted to the substrate due to the need to develop an SH mixture that can be applied to large constructions.

2. Materials and Methods

2.1. Required Materials. We developed an SH combination that uses polymer nanocomposite (PNC) strengthened with nanosized ZrO_2 nanoparticles and CS molecules to inhibit aluminum erosion in seawater. It is possible to alter the number of ZrO_2 nanoparticles incorporated in the PNC using PVC resin, a polymer binder. PVC resins are a water-insoluble material with suitable properties, including Young's modulus, shock absorbance, and chemical resistance for a corrosion-resistant coating. The ZrO_2 nanoparticles concentration supplied to the PVC matrix can be adjusted to improve the dried film's surface roughness. The surface energy of the composite is reduced by adding the reduced surface energy substance CS to the PVC matrix. The superhydrophobicity of the chosen polymer is a result of decreased surface energy and factors enhancing roughness. An AA-7475 aluminum alloy is used as a test specimen to determine the SH mixture's corrosion resistance. Ammonium hydroxide, zinc acetate, and copper sulfate are some ingredients that make up this mixture. By creating a coating resistant to corrosion for AA-7475 aluminum alloy, ZrO_2 nanoparticles (which adds roughness) and CS (which lowers surface energy) are mixed into polyvinyl chloride (PVC) binder. We have AA-7475 plates that are 60 mm long, 10 cm wide, and only half a millimeter thick. The surfaces are cleaned using ultrasonication and air dried to prepare the specimens for superhydrophobic (SH) combination.

2.2. Preparation of ZrO_2 Nanoparticles. Using the same easy precipitation method described in our previous research [26], ZrO_2 nanoparticles can be easily made. Simply 50 mL of distilled water was used to dissolve 0.05 M of sodium hydroxide and 0.01 M of Zn acetate. Drop by drop and rapidly agitated at 27°C, the zinc acetate is added to the sodium hydroxide solution until both solutions are neutralized. Zinc hydroxide begins to nucleate and develop, and white precipitate forms during stirring. After centrifuging, filtering, and rinsing with distilled water three times, the residue was dried in a hot air oven for 5 hr at 120°C. After drying, it is calcined for 1 hr at 700°C to produce ZrO_2 nanoparticles, which are then gathered and stored under a vacuum until needed.

2.3. Preparation of CS. The experimental method for preparing copper stearate (CS) is described in the literature [27]. In two different beakers, you'll dissolve 2.49 g of $CuSO_4$ (0.02 M) and 4.98 g of stearic acid (0.03 M) in 62 mm of water and 42 mm of ethanol, respectively. At 60°C for 30 min, while constantly stirring, they are heated in a water bath to combine the liquids. When NH_4OH was added, the mixture's pH raised to 7. After prolonged stirring, a vivid blue precipitate was obtained; this was then systematically washed and filtered using a mixture of distilled water and ethanol at a 1 : 1 ratio. This residue was stored in an airtight container after air-drying.

2.4. Fabrication of Polymer Nanocomposites. ZrO_2 nanoparticles and CS are bound to create SH material using polyvinyl

Table 1: The PVC matrix contains ZrO_2 nanoparticles and CS compositions.

Polymer nanocomposites	ZrO_2 nanoparticles (g)	CS	PVC (g)	THF (mL)
PNC-1 (Sample-1)	0.30	1	0.30	60
PNC-2 (Sample-2)	0.60	1	0.30	60
PNC-3 (Sample-3)	0.90	1	0.30	60
PNC-4 (Sample-4)	1.20	1	0.30	60
PNC-5 (Sample-5)	1.50	1	0.30	60

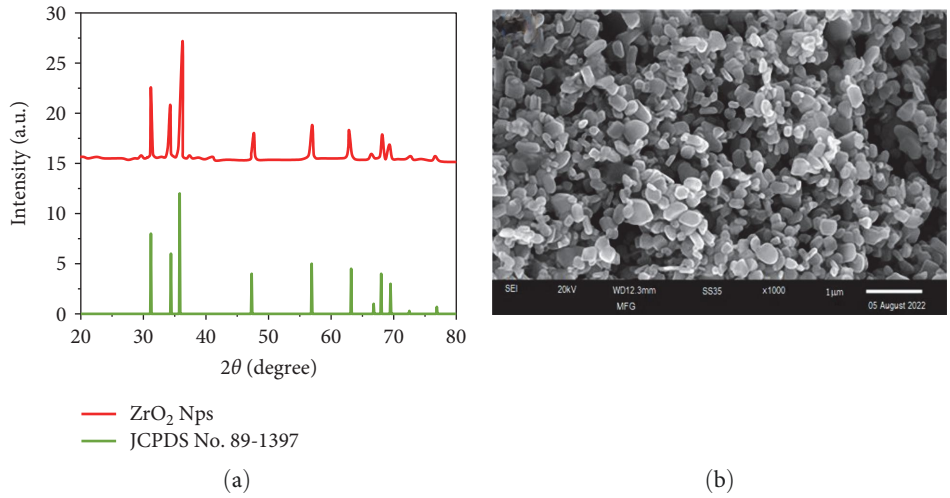

Figure 1: (a) XRD pattern and (b) FESEM image.

chloride (PVC). THF is first used to dissolve 0.30 g of PVC (0.6 wt%), trailed by adding 1 g of CS (2 wt%), which is agitated while the mixture is stirred. After the mixture is uniform, different amounts of ZrO_2 nanoparticles are added, such as 0.30, 0.60, 0.90, 1.20, and 1.50 g, for weight percentages of 0.6, 1.2, 1.8, 2.4, and 3.0, respectively (Table 1). Sonicating the mixture with a probe-type ultrasonicator produces a homogeneous suspension of ZrO_2 nanoparticles in PVC. Sonication was performed for 30 min, with on-and-off intervals of 30 s each. After sonication, the mixture is degassed in a desiccator at a lower pressure of 0.2 bar for 20 min to reduce the impact on air spaces. After the AA-7475 samples have been ultrasonically cleaned, they are brush coated with the resulting mixture, allowed to air dry for 24 hr, and then kept until further characterization [28, 29].

2.5. Description. This ZrO_2 nanoparticles sample's X-ray diffraction (XRD) pattern was measured using a Siefert XRD with Cu-Kα radiation at a wavelength of $\lambda = 1.5406$ Å and $a = 20°$–$80°$. The molecular vibrations of PNCs are recorded using an IR spectrometer. Field-emission scanning electron microscopy (FESEM) reveals the ZrO_2 nanoparticles' morphological features. To determine the average roughness of the 3D atomic force microscope (AFM), the XE-70 AFM's topographical line profile analysis is used [30]. After 30 s of immersion in 10 L of water, a goniometer measures the coated surfaces' WCA. Potentiodynamic polarization (PDP) and electrochemical impedance experiments in a 3.5% NaCl solution were used to evaluate the SH coating produced by CH instruments for corrosion resistance.

3. Results and Discussion

It is necessary to increase the surface roughness of PNC by using wet, chemically produced ZrO_2. It depicts the XRD structure of the ZrO_2 nanoparticles produced in the range of 20°–80° in Figure 1(a). There are well-defined crystallization patterns in the $2\theta = 31.7488°$, 34.4094°, 36.2346°, 47.5557°, 56.5974°, 62.8460°, 66.4176°, 67.9315°, 69.0682°, 72.5721°, and 77.0375° peaks in the XRD spectrum. Peaks (100, 002, 101, 102, 110, 103) are good match for JCPDS No. 89-1397 (Figure 1(a)). A tetrahedral hexagonal wurtzite phase of ZrO_2 nanoparticles features Zn^{2+} ringed by four O_2 molecules. For the ZrO_2 nanoparticles were created, Scherer's formula [31] was used to calculate the average crystallite size.

$$D = 0.9\lambda/(\text{FWHM} \times \cos\theta). \quad (1)$$

The FWHM is the whole breadth at half-maximal of the deflected peak, and θ is the XRD angle. ZrO_2 nanoparticles have a crystallite size of 40 nm, according to the formula above. ZrO_2 nanoparticles defects are to blame for the deviation from the conventional values of 3.253 Å, 5.213 Å, and 47.77 3 $Å^3$ for the lattice parameters a to c, and volume of the

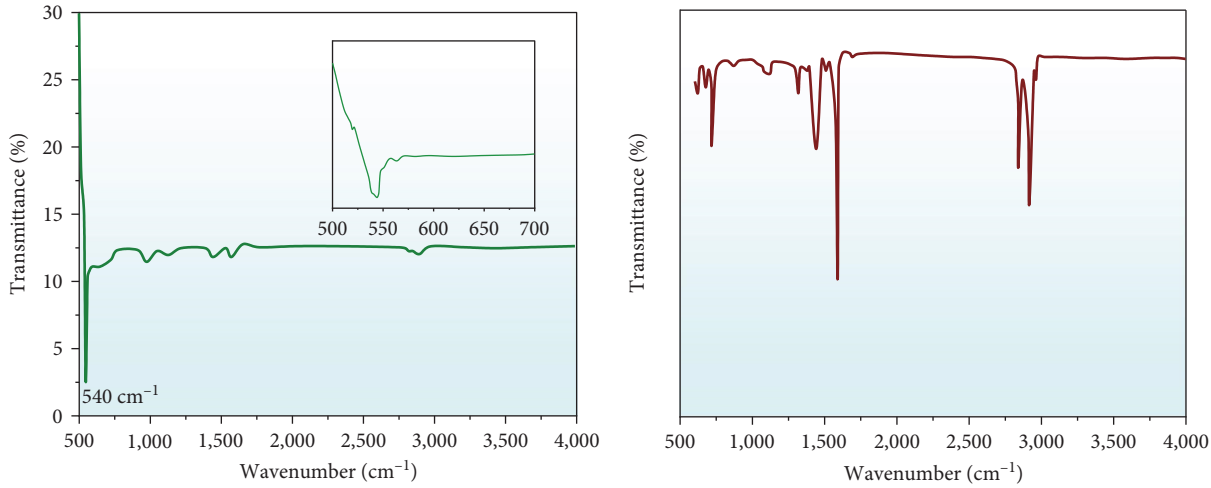

Figure 2: (a) Fourier-transform infrared spectrum of ZrO_2 nanoparticles and (b) CS.

ZrO_2, which are 3.24915 Å, 5.20673 Å, and 47.6031 3 Å^3 correspondingly.

ZrO_2 nanoparticles secondary electron FESEM image as shown in Figure 1(b). The ZrO_2 nanoparticles structures depicted in the figure range in size from 100 to 200 nm and are polydispersed. The ZrO_2 nanoparticles have a highly crystalline character, confirming the results of XRD.

Figure 2(a) shows the Fourier-transform infrared spectra of ZrO_2 nanoparticles produced between 500 and 4,000 cm^{-1}. ZrO_2 vibrational has highest at 540 cm^{-1} in extended-spectrum shown in Figure 2(a). Copper precursor ions easily react with $CH_3(CH_2)16COO^-$ ions in stearic acid during the CS synthesis in the occurrence of ethanol, resulting in Cu $(CH_3(CH_2)16COO)_2$ molecules. An illustrated in Figure 2(b), which depicts the characteristic molecular vibrational patterns of each of its elements. Stearic acid's distinctive stretching frequency (1,512–1,520 cm^{-1}) has vanished from Figure 2(b). The carboxylate group produced by the interaction of stearic acid with the metal precursor resulted in a strong signal at 1,762 cm^{-1}. The aliphatic C–H stretching frequencies of the CS molecule are 2,846 and 2,910 cm^{-1}, respectively. Vibrations in the 1,441 and 717 cm^{-1} range for C–C and C–H show bending and asymmetric stretching.

ZrO_2 nanoparticles of 0.6, 1.2, 1.8, 2.4, and 3.0 are distributed with 2.4 wt% copper stearate and various weight percentages of ZrO_2 nanoparticles (PNC-1 to PNC-5) in THF at a concentration of 0.6 wt%. The spectrum of PNC in the region of 500–4,000 cm^{-1} is shown in Figure 3 (right). The distinctive ZrO_2, CS, and PVC bands were seen in all spectra. The peak of the Zn–O vibrations can be located at 520 cm^{-1}, and its intensity increases as ZrO_2 nanoparticles wt% increases. Spectral peaks in the 500–1,500 cm^{-1} range suggest the presence of PVC. All of the PVC stretching processes are attributed to the peaks at 1,306 cm^{-1} (–CH scissoring of PVC), 1,433, 2,856 cm^{-1}, and CH asymmetric stretching of polyvinyl chloride.

With this research, we hope to create an AA-7475 corrosion-resistant coating with a superhydrophobic characteristic. Roughening components and low surface energy are

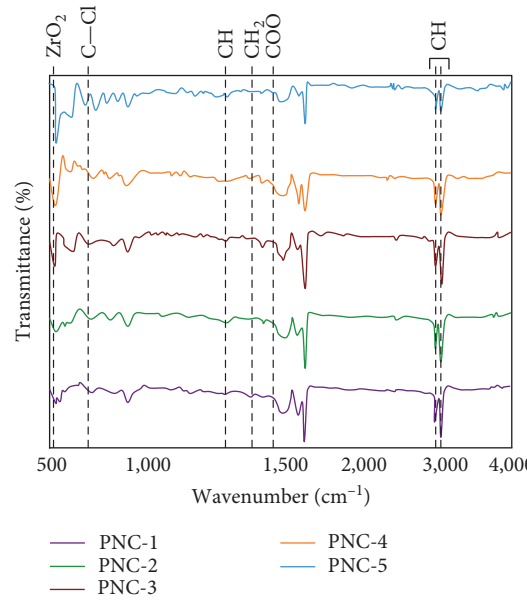

Figure 3: Fourier-transform infrared spectrum of polynanocomposites: (a) Sample-1, (b) Sample-2, (c) Sample-3, (d) Sample-4, and (e) Sample-5.

combined to form a superhydrophobic surface with a WCA of more than 150° PVC binder in THF solvent blended with roughening components. WCA of coating, which is made of ZrO_2 nanoparticles and CS in PVC, has been improved by using this material. The bigger the number of ZrO_2 nanoparticles in the coating, the greater the WCA. Line profile analysis is a valuable technique in the software used to interpret pictures to evaluate the coating surface roughness. Using a WCA, the surface roughness (Ra) of the PNC-1 was determined to be 12.74 nm at an angle WCA of 124°, as indicated in Figure 4(a). ZrO_2 nanoparticles wt% is increased from 0.6 to 1.2, although the WCA only increases by 128° (Figure 4(b)). WCA is not significantly improved because the difference in Ra is just

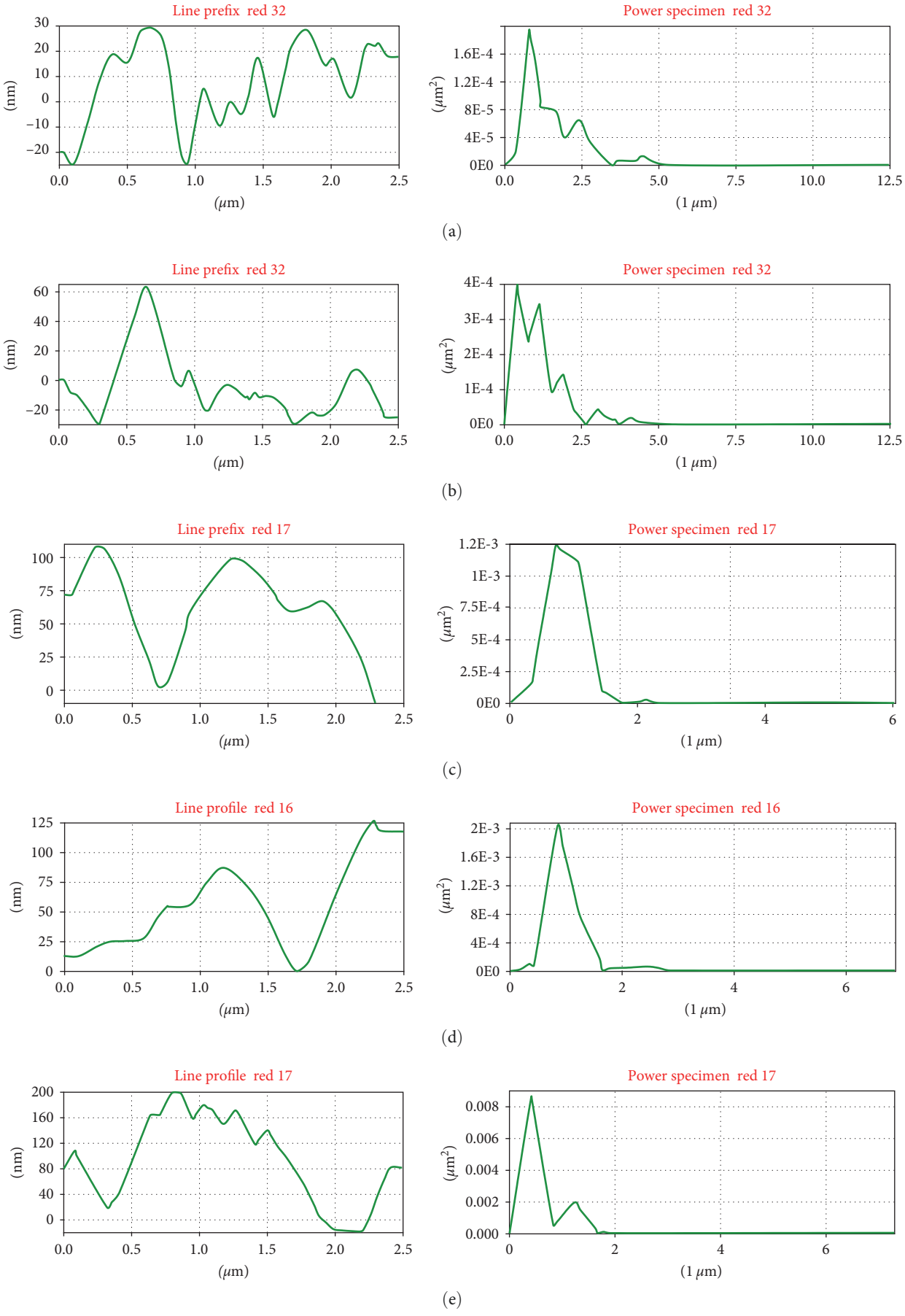

Figure 4: Line profile analysis of polymer nanocomposites: (a) Sample-1, (b) Sample-2, (c) Sample-3, (d) Sample-4, and (e) Sample-5.

Table 2: Mean roughness and WCA of polymer nanocomposites.

Polymer nanocomposites	ZrO_2 nanoparticles (wt%)	Avg. roughness (nm)	WCA (°)
PNC-1 (Sample-1)	0.6	11.82	125
PNC-2 (Sample-2)	1.2	15.36	126
PNC-3 (Sample-3)	1.8	25.81	134
PNC-4 (Sample-4)	2.4	29.96	136
PNC-5 (Sample-5)	3.0	60.52	154

WCA, water contact angle.

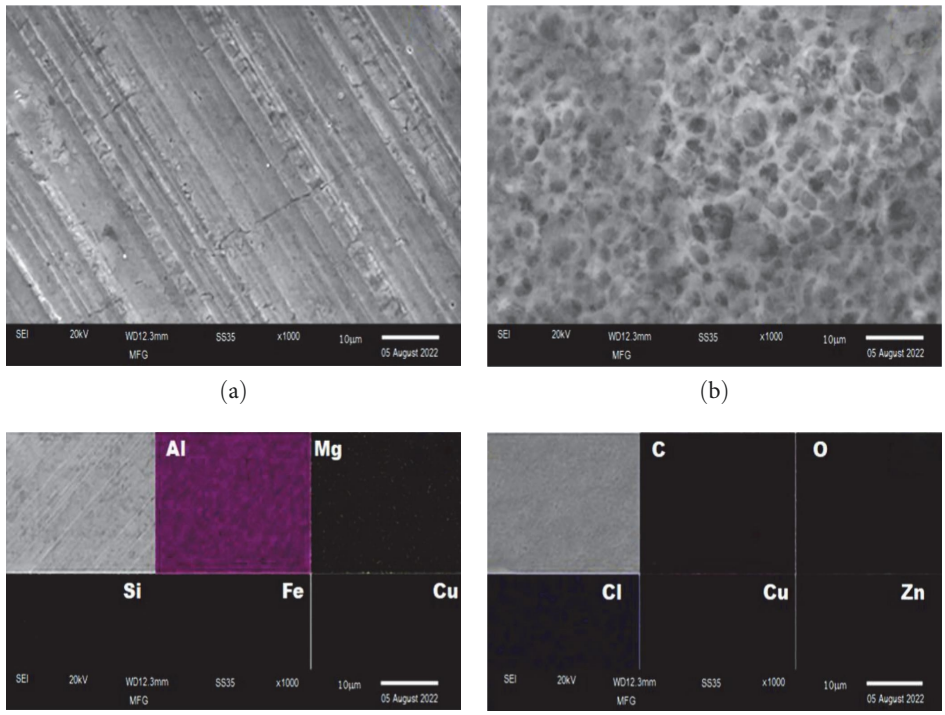

Figure 5: (a, b) SEM and (c, d) EDX mapping images of bare and PNC-5-coated AA-7475.

16.47 nm. With ZrO_2 nanoparticles content rising to 1.8 and 2.4 wt%, the roughness value rises to 26.72 and 30.90 nm in PNC-3 and PNC-4 accordingly (Figures 4(c) and 4(d)). Ra values have increased. However, WCA does not reach superhydrophobic (about 150°) levels despite this. It turns out that the Ra value is double for PNC-4 when 3.0 wt% of ZrO_2 nanoparticles (PNC-5) is added. This PNC-5 coating is classified as SH because of its 154° WCA on such a roughened surface.

These results indicate a strong correlation between roughness and SH activity, forming comparable nanoscale pillars [32]. Due to its hierarchical structure, air molecules are trapped between valleys and peaks of the PNC covering [33]. The Cassie–Baxter model is a good fit for these SH surface phenomena.

$$\cos\theta_{CB} = f_{ls}\ \cos\theta_0 - f_{lv}, \tag{2}$$

where θ_{CB} is the WCA of PNCs, θ_0 is Young's angle of contact, f_{ls} and f_{lv} divides the projected area by the contact region between liquid and solid and liquid and vapor. Surface roughness is a crucial aspect that contributes to creating SH surfaces in the current scenario. As a result, Peng et al. [34] is substituted into the equation,

$$\cos\theta_{CB} = r_f f\ \cos\theta_0 - f - 1, \tag{3}$$

where r_f is the surface roughness, and f is the percentage of a solid surface covered by water. There are varied ZrO_2 nanoparticle concentration percentages in Table 2 for PNC-1 to 5.

PNC-5-coated AA-7475 exhibits a WCA of 154°, indicating that it has a superhydrophobic coating, as may be deduced from Table 2. When it comes to corrosion protection, the PNC coated with AA-7475 alloy serves this purpose.

Images of AA-7475 coated with PNC-5, as shown in Figures 5(c) and 5(b). Figure 5(a) depicts the AA-7475 surface morphology without any holes. Porous structures are formed on the surface of PNC-5 when it is applied. The ZrO_2 nanoparticles induce the coating's roughness, and the porous structure may have been formed due to the coating's presence of CS [31, 35]. The porous structure of the coating's

Table 3: Details of corrosion parameters obtained from potentiodynamic polarization studies.

Sample	Corrosion potential E_{corr} (V)	Pitting corrosion potential E_{pit} (V)	Corrosion current density i_{corr} (A)	Protective efficiency (%)	Corrosion rate v_{corr} (mpy)
Bare AA-7475	−1.260	−0.676	5.536×10^{-5}	–	2.376×10^{1}
PNC-5-coated AA-7475	−0.397		5.362×10^{-7}	99.06	2.252×10^{1}

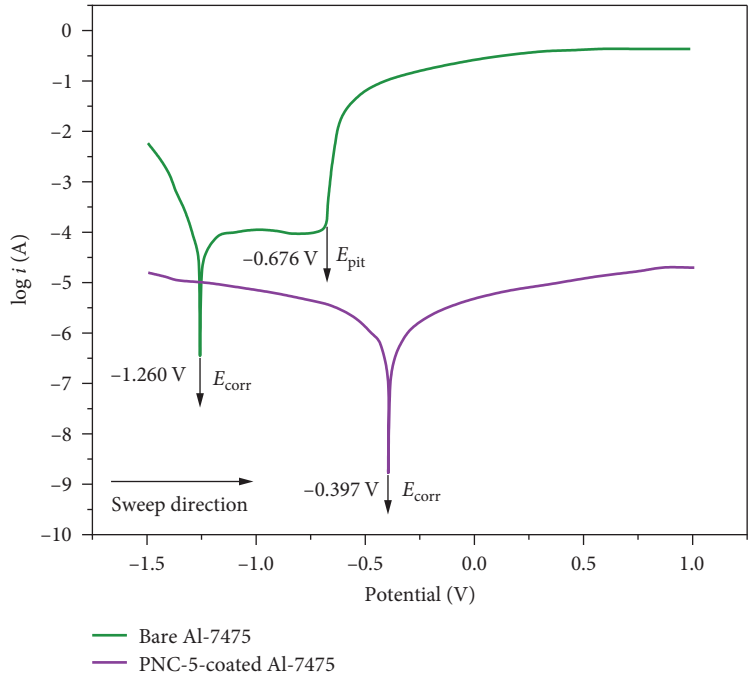

Figure 6: Potentio-dynamic polarization studies of (a) bare and (b) PNC-5-coated AA-7475.

surface may be responsible for the greater WCA. Figures 5(c) and 5(d) show the EDX mapping of the AA-7475 coated with PNC-5 and naked samples. ZrO_2 and CS were found to be present. Elemental maps of AA-7475 show a high concentration (>99%) of Al, although there are also trace amounts of Mg and Si and Fe, and Cu, as well as other elements. The alloying ingredients in AA-7475 are thought to be responsible for the trace element presence [36]. PVC matrix constituents C, O, and Cl can be seen on the surface of AA-7475 coated with PNC-5 (Figure 5(d)). For this reason, trace amounts of zinc, copper, and other metals can be found in the completed product. Since Zn and Cu atoms are uniformly distributed across the PNC-5 surface, this supports the presence of ZrO_2 nanoparticles and CS.

The corrosion resistance of superhydrophobic PNC-5 coated and uncoated Aluminum-7475 specimens are studied using PDP and electrochemical impedance spectroscopy (EIS) investigations. The cathode uses the electrons released by the oxidation reaction on the working electrode's surface to perform the reduction. The following is a list of aluminum corrosion reactions:

$$\mathrm{Al} \longrightarrow \mathrm{Al}^{3+} + 3e^{-}, \tag{4}$$

$$\mathrm{O_2} + 2\mathrm{H_2O} + 4e^{-} \longrightarrow 40\mathrm{H}^{-}, \tag{5}$$

$$\mathrm{Al}^{3+} + 3\mathrm{OH}^{-} \longrightarrow \mathrm{Al(OH)_3}, \tag{6}$$

$$2\mathrm{Al(OH)_3} + \text{in air} \longrightarrow \mathrm{Al_2O_3} \cdot 3\mathrm{H_2O}. \tag{7}$$

Anode Al atoms consume the hydroxide ions produced on the cathode, resulting in aluminum hydroxide, which is then transformed into an aluminum oxide coating by the anode. A barrier between hydroxides and our substrates can prevent the formation of oxide layers. A layer of SH material is applied to the AA-7475 to shield the substrate from direct contact with the electrolyte [37]. The resulting specimen is used as a counter and a reference electrode because platinum and Ag/silver chloride are both acceptable electrode materials [38, 39]. All tests are conducted with a marine-like electrolyte solution of 3.5% NaCl. Samples are stabilized in 3.5% sodium chloride for an hour before electrochemical tests are conducted and the open circuit potential is determined.

Aluminum-7475 (ASTM standard) was bare and coated with PNC-5 at a scan rate of 0.1667 mV/s to estimate corrosion potential (E_{corr}), corrosion current density (i_{corr}), polarization resistance (R_p), (i'_{corr}) corrosion current density of AA-7475 and other electrochemical parameters. These samples' corrosion behavior may be estimated and summarized in Table 3 using anodic and cathodic polarization curves, which are shown in Figure 6. PNC-5 was shown to reduce the corrosion resistance of AA-7475 from 5.536×10^{-5} A to

Table 4: Resistance data in the linear polarization direction.

Specimen	Slope at anode b_a	Slope at cathode b_c	Corrosive current density i_{corr} (A)	Polarized resistance R_p (Ω·cm^2)
Bare AA-7575	2.370	11.341	5.538×10^{-5}	14.135×10^3
PNC-5-coated AA-7475	5.031	5.524	5.253×10^{-7}	20.682×10^5

5.253×10^{-7} A, based on the data in Table 3. When aluminum-7475 was stacked on top of PNC-5, the E_{corr} voltage dropped from −1.260 to −0.397 V after coated, with a positive shift of 0.863 V. The superhydrophobic surface produced with PNC-5 effectively shields the metallic surface from corrosion, preventing electrolytes from penetrating toward working electrodes, as seen by the decrease in i_{corr} and increased E_{corr} values. AA-7475 surfaces are protected from erosion by limiting hydroxide generation. To assess the PNC-5 coating's level of protection, apply the following formula to estimate P_i:

$$P_i(\%) = [1 - (i_{corr}/i'corr)] \times 100. \quad (8)$$

Samples coated with PNC-5 had a P_i that is 99.05% corrosion-resistant. Corrosion rates (mpy) of AA-7475 coated and uncoated can be determined using the formula [29].

$$v_{corr} = \frac{i_{corr} K E_w}{\rho A}, \quad (9)$$

where E_w is the metal's equivalent weight to be tested for corrosion rate, K is a constant that measures 1.288×10^{-5}, ρ is a representation of metal density, and A, which metal surfaces in a PDP sample were immersed in the conductive electrolyte during the test. AA-7475 corrosion rate is 23.75 mpy, but PNC-5-layered AA-7475 is 0.2253 mpy, which is 100 times less corrosion-resistant.

In this case, the pitting corrosion is responsible for the appearance of the hump at −0.675 V, which can be seen in a typical PDP pattern on bare Al. The damaged aluminum reacts with the electrolyte at higher anodic ranges, forming aluminum salts and a pit in the specimen. "Pitting potential" refers to that point in developing a pit where further development is possible (Epit). During exposure to high Cl concentrations, localized corrosion creates microscopic holes in the aluminum surface, leading to pitting [40]. A small region acts as an anode for the heavy corrosion that produces small pits, influencing pitting corrosion. The start, metastable development, and stable, autocatalytic growth stages of pit formation are described by Chang et al. [41]. To avoid pitting, an appropriate coating must be applied to the areas that are susceptible to pitting, according to their findings. The breakdown of aluminum in a chloride-rich atmosphere causes pitting corrosion.

$$Al = Al^{3+} + 3e^-, \quad (10)$$

$$Al^{3+} + 4Cl^- = AlCl_4^-. \quad (11)$$

Figure 5 demonstrates that the naked AA-7475 is pitting corroded at a potential of −0.676 V. However, the sample does not reveal any peak matching to Epit when coated with superhydrophobic material, i.e., PNC-5. When an AA-7475 surface is coated with a PNC-5 electrolyte solution and cannot migrate into the interior, anodic and cathodic islands are prevented from forming. 3.5% NaCl solution did not produce pits when PNC-5 was applied as the protective coating.

For the bare and coated AA-7475, the polarization resistance (R_p) was calculated using an equation based on Stern–Geary [42].

$$R_p = \frac{B}{i_{corr}}, \quad (12)$$

$$B = \frac{b_a b_c}{2.3(b_a + b_c)}, \quad (13)$$

where b_a and b_c slopes of the anodic and cathodic conductors. Table 4 contains the values of R_p and various other factors. The results reveal that coating PNC-5 over AA-7475 enhances b_a while decreasing b_c, demonstrating that corrosion slowed in the coated specimens. As a result, the coated sample has a higher R_p ($21.682 \times 10^3\ \Omega$·cm^2) than the bare AA-7475 ($15.135 \times 103\ \Omega$·cm^2). It has been determined that the SH coating on the PNC-5 provides adequate corrosion protection in a maritime environment based on PDP data.

EIS analysis can determine electron transfer mechanisms between the working electrolyte and the electrode. Recordings of PNC-5 coated aluminum-7475 in 3.5% sodium chloride solutions were plotted in Figure 7 from 0.01 to 100,000 Hz. The R_{ct} of the specimens is measured using a capacitive loop at high frequencies. As demonstrated in Table 5, the coated specimen has an R_{ct} value of $2.598\ \Omega$·cm^{-2}, which is significantly greater than the untreated sample R_{ct} value of $51.29\ \Omega$·cm^{-2}.

As displayed in Figure 7(c), bode charts of magnitude and phase angle can be seen in both naked and PNC-5-coated samples. The PNC-5-coated sample demonstrated a higher impedance than the bare AA-7475 in all frequency bands. For bare AA-7475, plotting the phase angle shows only one-time constant of roughly ∼50 Hz, owing to the oxide coating produced on the Al surface. The maximum frequency (∼1,000,000 Hz) can increase by increasing the time constant of PNC-5-coated AA-7475. The AA-7475 surface has been protected from corrosion by the PNC-5 coating, which has altered the time constant significantly. For evaluating electrochemical parameters through curve fitting, we can use the EEC model for the Nyquist plot (Figure 7(d)). Table 5 shows the calculated values for the circuit parameters, which indicate solution resistance, resistance to charge transfer two-layer capacitance, and the Warburg factor. While AA-7475 with no PNC-5 coating has an R_s of just $2.974\ \Omega$, the PNC-5-coated AA-7475 has an R_s of $7.187\ \Omega$

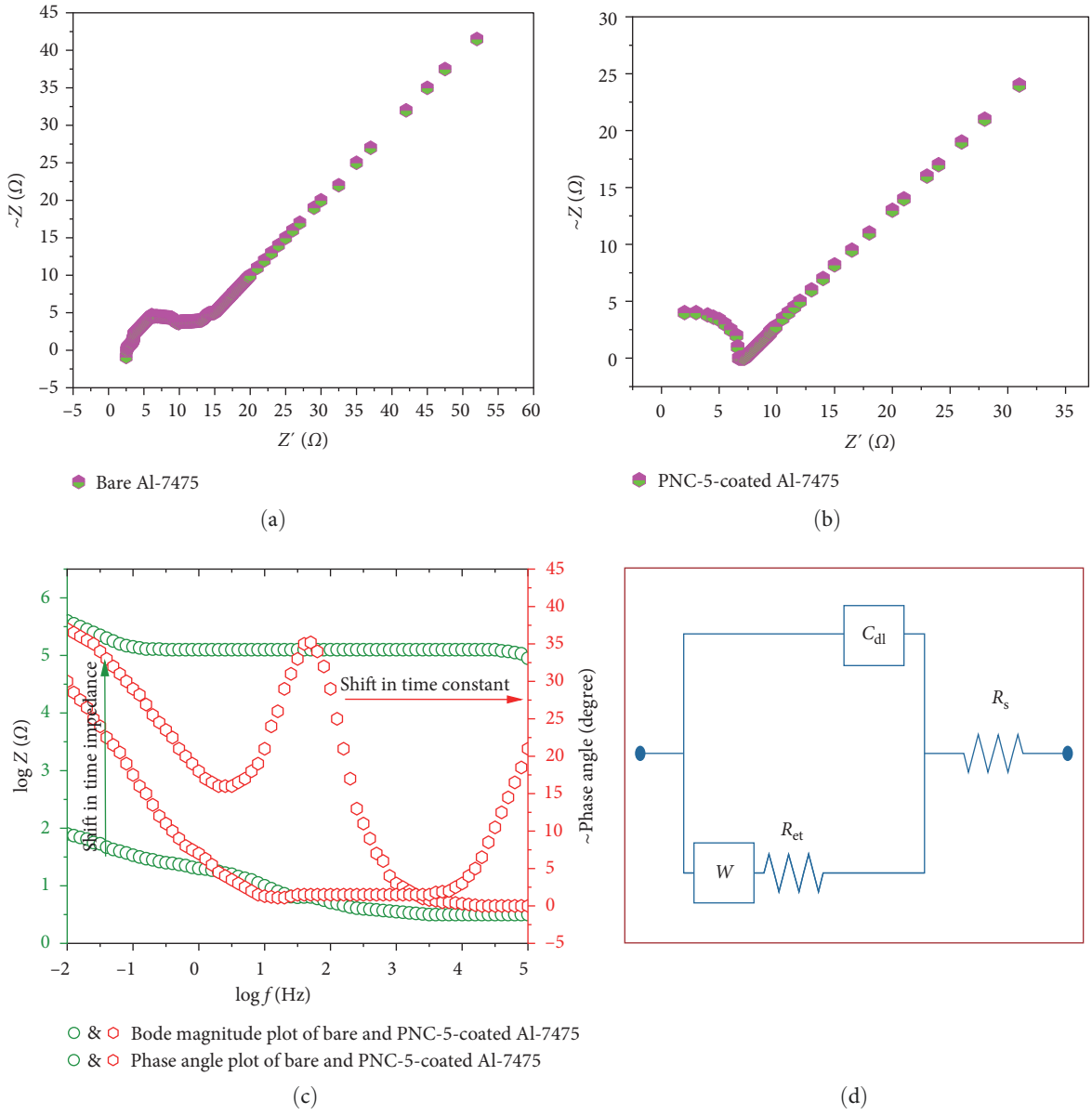

Figure 7: (a) Nyquist plot for bare AA-7475, (b) polymer nanocomposites-5 coating with AA-7475 (c) magnitude plot and phase angle (d) equivalent circuit.

Table 5: Equivalent circuit data.

Specimen	R_s (Ω)	R_{et} (Ω·cm^2)	C_{dl} (F·cm^2)	W
Bare AA-7475	2.974	51.79	7.05×10^{-4}	6.290×10^{-2}
PNC-5-coated AA-7475	7.187×10^{4}	2.598×10^{5}	3.932×10^{-11}	1.748×10^{-5}

by the same order of magnitude. An increase in R_s has been attributed to an air-trapping phenomenon that successfully repels the electrolyte from PNC-5-coated samples because of their SH composition. This indicates that the PNC-5-coated AA-7475 is an excellent conductor of electricity between metallic surfaces and electrolytes because it has the highest C_{dl}, compared to bare aluminum [43]. It also shows that the creation of compound W successfully limits the flow of electrons in an electrochemical circuit. According to these data, corrosion of AA-7475 is prevented by PNC-5's SH surface.

Figure 8(a)–8(d) shows before and after PDP measures on AA-7475 coated with PNC-5 and bare AA-7475 using scanning electron microscopy (SEM). According to the SEM picture in Figure 8(a), the AA-7475 surface is completely noncorrosive

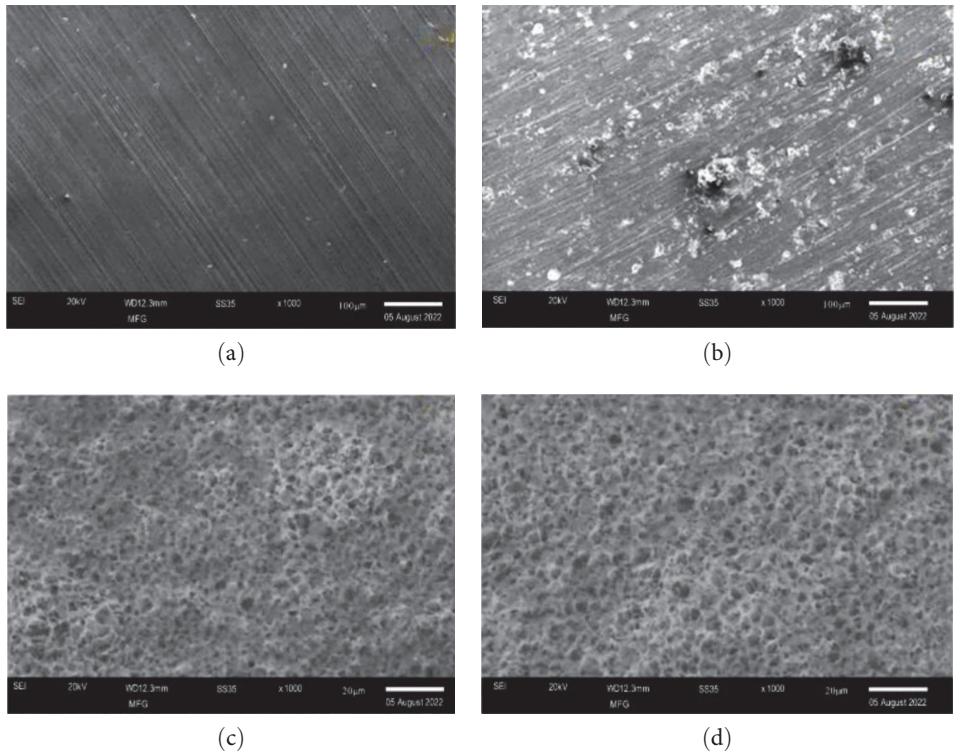

Figure 8: SEM image of bare and PNC-5-coated AA-7475 before (a, c) and after (b, d) potentiodynamic polarization studies.

(Figure 8(a)). However, after PDP examinations, the surface is eroded, with pits forming on all of its surfaces, confirming the conclusions of the PDP graph. No cracks or delaminations were found on the AA-7475 coated with PNC-5 compared to AA-7475 untreated as a control. An unbroken and undamaged PNC-5 shows that the underlying AA-7475 (Figures 8(a) and 8(d)) has been completely protected.

An X-cut tape testing, performed by ASTM D 3359-96.4 cm X-cut on a layer of the angle at 30°, is used to determine the observance of the PNC-5 coating. The X-cut region is covered with adhesive tape and left for 60 s. During the 60 s, an adhesive tape is applied and left in place on the X-cut area. During the first 60 s of peeling, the peeling angle should be close to 180°. The coating is classified as 5 A denotes the absence of peeling, and 0 A denotes the removal of coating from the substrate. Using a screw gauge, the coating thickness is determined to be 160 μm.

4. Conclusion

(i) To create a superhydrophobic polymer, nanocomposite PVC, copper stearate, and ZrO_2 are mixed in the right proportions. Changing the weight percentage of ZrO_2 nanoparticles to 0.6, 1.2, 1.8, 2.4, and 3.0 wt% allows researchers to investigate the impact of average roughness on SH behavior.

(ii) According to the WCA data, the PNC (PNC-5) included in the 3.0 wt% ZrO_2 nanoparticles exhibits SH character. The average roughness of the coating has been found to significantly impact the SH surface from the line profile analysis of the AFM picture. After brush coating, an AA-7475 substrate with the SH PNC-5 combination, electrochemical workstations assess corrosion resistance in a 3.5% NaCl.

(iii) As a result of these findings, the PNC-5-coated A1-7475 has a higher $E_{corr} = 0.397$ V, the lowest $i_{corr} = 5.513 \times 10^{-7}$ A, the smallest V_{corr} is 0.2254 mpy, and a higher $R_p = 21.682 \times 10^5\,\Omega{\cdot}cm^2$ than bare AA-7475 ($E_{corr} = -1.260$ V, $i_{corr} = 5.513 \times 10^{-5}$ A, $v_{corr} = 23.76$ mpy, and $R_p = 21.682 \times 10^5\,\Omega{\cdot}cm^2$. Because of the nanocomposite's SH property, pitting corrosion in PNC-5 high corrosion-resistant performance on AA-7475 alloy is greatly reduced.

Data Availability

The data used to support the findings of this study are included within the article.

Conflicts of Interest

The authors declare that they have no conflicts of interest.

References

[1] X. Cao, X. Sun, S. Xiao, G. Cai, X. Zhang, and Z. Dong, "Preparation and anti-wearing and anticorrosion properties of 3D superhydrophobic coating based on poly-benzoxazine," *Acta Materiae Compositae Sinica*, vol. 39, no. 2, pp. 617–627, 2022.

[2] A. S. Sarkın, N. Ekren, and Ş. Sağlam, "A review of anti-reflection and self-cleaning coatings on photovoltaic panels," *Solar Energy*, vol. 199, pp. 63–73, 2020.

[3] J. Kujawa, "From nanoscale modification to separation—the role of substrate and modifiers in the transport properties of ceramic membranes in membrane distillation," *Journal of Membrane Science*, vol. 580, pp. 296–306, 2019.

[4] X. Yu, L. An, J. Yang, S.-T. Tu, and J. Yan, "CO_2 capture using a superhydrophobic ceramic membrane contactor," *Journal of Membrane Science*, vol. 496, pp. 1–12, 2015.

[5] M. Tuominen, H. Teisala, J. Haapanen et al., "Adjustable wetting of liquid flame spray (LFS) TiO_2-nanoparticle coated board: batch-type versus roll-to-roll stimulation methods," *Nordic Pulp & Paper Research Journal*, vol. 29, no. 2, pp. 271–279, 2014.

[6] E. Nyankson, H. Agbe, G. K. S. Takyi, Y. D. Bensah, and D. K. Sarkar, "Recent advances in nanostructured superhydrophobic surfaces: fabrication and long-term durability challenges," *Current Opinion in Chemical Engineering*, vol. 36, Article ID 100790, 2022.

[7] A. Jagtap, P. G. Wagle, E. Jagtiani, and A. P. More, "Layered double hydroxides (LDHs) for coating applications," *Journal of Coatings Technology and Research*, vol. 19, pp. 1009–1032, 2022.

[8] Y. Cheng, X. Zuo, X. Yuan et al., "Preparation of fluorine silicon copolymer superhydrophobic anticorrosive coating on copper aluminium composite by one step spraying," *Materials Letters*, vol. 304, Article ID 130496, 2021.

[9] H. Zheng, Z. Li, L. Liu, F. Meng, Y. Cui, and F. Wang, "Superhydrophobic composite coatings in bacterial culture media: durable antibacterial activity and enhanced corrosion resistance," *Composites Communications*, vol. 27, Article ID 100857, 2021.

[10] W. Wang, "Preparation of new polymer nanocomposites and analysis of their superhydrophobic properties," *IOP Conference Series: Earth and Environmental Science*, vol. 714, Article ID 032072, 2021.

[11] M. S. Selim, S. A. El-Safty, M. A. Abbas, and M. A. Shenashen, "Facile design of graphene oxide-ZnO nanorod-based ternary nanocomposite as a superhydrophobic and corrosion-barrier coating," *Colloids and Surfaces A: Physicochemical and Engineering Aspects*, vol. 611, Article ID 125793, 2021.

[12] T. Ning, W. Xu, and S. Lu, "Fabrication of superhydrophobic surfaces on zinc substrates and their application as effective corrosion barriers," *Applied Surface Science*, vol. 258, no. 4, pp. 1359–1365, 2011.

[13] C. H. Lee, J. Drelich, and Y. K. Yap, "Superhydrophobicity of boron nitride nanotubes grown on silicon substrates," *Langmuir*, vol. 25, no. 9, pp. 4853–4860, 2009.

[14] R. B. Jeen Robert, G. S. Hikku, K. Jeyasubramanian, J. Jacobjose, and R. Malkiya Rasalin Prince, "ZnO nanoparticles impregnated polymer composite as superhydrophobic anticorrosive coating for Aluminium-6061 alloy," *Materials Research Express*, vol. 6, no. 7, Article ID 075705, 2019.

[15] A. Barhoum, J. Jeevanandam, and M. K. Danquah, *Fundamentals of Bionanomaterials*, Elsevier, 2022.

[16] C. C. Ong, R. Jose, and M. S. M. Saheed, "Atomic defects of graphene-carbon nanotubes impact on surface wettability," *Applied Surface Science*, vol. 567, Article ID 150803, 2021.

[17] S. G. V. Kumar, P. Prabhakar, R. K. Sen, N. Uppal, M. A. Khan, and A. K. Srivastava, "Development of superhydrophobic cotton fabric using zinc oxide nanoflower/polydimethylsiloxane (PDMS) nanocomposite coatings," *Textile & Leather Review*, vol. 4, no. 4, pp. 253–266, 2021.

[18] S. Ghosh, B. Nitin, S. Remanan et al., "A multifunctional smart textile derived from merino wool/nylon polymer nanocomposites as next generation microwave absorber and soft touch sensor," *ACS Applied Materials & Interfaces*, vol. 12, no. 15, pp. 17988–18001, 2020.

[19] F. Gao, J. Mu, Z. Bi, S. Wang, and Z. Li, "Recent advances of polyaniline composites in anticorrosive coatings: a review," *Progress in Organic Coatings*, vol. 151, Article ID 106071, 2021.

[20] B. Yin, T. Xu, D. Hou et al., "Superhydrophobic anticorrosive coating for concrete through in-situ bionic induction and gradient mineralization," *Construction and Building Materials*, vol. 257, Article ID 119510, 2020.

[21] X. Yin, P. Mu, Q. Wang, and J. Li, "Superhydrophobic ZIF-8-based dual-layer coating for enhanced corrosion protection of Mg alloy," *ACS Applied Materials & Interfaces*, vol. 12, no. 31, pp. 35453–35463, 2020.

[22] V. Sharma, V. Sharma, M. S. Goyat et al., "Recent progress in nano-oxides and CNTs based corrosion resistant superhydrophobic coatings: a critical review," *Progress in Organic Coatings*, vol. 140, Article ID 105512, 2020.

[23] Z. Yang, X. Liu, and Y. Tian, "A contrastive investigation on anticorrosive performance of laser-induced super-hydrophobic and oil-infused slippery coatings," *Progress in Organic Coatings*, vol. 138, Article ID 105313, 2020.

[24] S. Ibrahim and M. Sultan, "Superhydrophobic coating polymer/silica nanocomposites: part I synthesis and characterization as eco-friendly coating," *Silicon*, vol. 12, pp. 805–811, 2020.

[25] Y. K. Hefni, "Hydrophobic zinc oxide nanocomposites for consolidation and protection of quartzite sculptures: a case study," *Journal of Nano Research*, vol. 63, pp. 64–75, 2020.

[26] C. Anitha, S. Syed Azim, S. Arunkumar, and S. Mayavan, "One pot fabrication of superhydrophobic anticorrosive coating without fluoro compounds and inhibitive pigments," *Progress in Organic Coatings*, vol. 125, pp. 137–145, 2018.

[27] R. Ramachandran and M. Nosonovsky, "Coupling of surface energy with electric potential makes superhydrophobic surfaces corrosion-resistant," *Physical Chemistry Chemical Physics*, vol. 17, no. 38, pp. 24988–24997, 2015.

[28] W. F. Huang, Y. L. Xiao, Z. J. Huang et al., "Super-hydrophobic polyaniline-TiO_2 hierarchical nanocomposite as anticorrosion coating," *Materials Letters*, vol. 258, Article ID 126822, 2020.

[29] E. Cho, S. H. Kim, M. Kim, J.-S. Park, and S.-J. Lee, "Superhydrophobic and antimicrobial properties of Ag-PPFC nanocomposite thin films fabricated using a ternary carbon nanotube-Ag-PTFE composite sputtering target," *Surface and Coatings Technology*, vol. 370, pp. 18–23, 2019.

[30] I. Sulym, A. Kubiak, K. Jankowska et al., "Superhydrophobic MWCNTs/PDMS-nanocomposite materials: Preparation and characterization," *Physicochemical Problems of Mineral Processing*, vol. 55, no. 6, pp. 1394–1400, 2019.

[31] K.-C. Chang and J.-M. Yeh, "Electroactive polymer-based anticorrosive coatings," in *Intelligent Coatings for Corrosion Control*, pp. 557–583, Butterworth-Heinemann, 2015.

[32] M. Akhavan, I. Hejazi, J. Seyfi et al., "Investigating the effect of surface composition and morphology on oil/water separation efficiency of sponges coated with polymer nanocomposites," *Polymer Composites*, vol. 40, no. S1, pp. e431–e439, 2019.

[33] T. Zhai, Q. Zheng, Z. Cai, L.-S. Turng, H. Xia, and S. Gong, "Poly (vinyl alcohol)/cellulose nanofibril hybrid aerogels with an aligned microtubular porous structure and their composites with

polydimethylsiloxane," *ACS Applied Materials & Interfaces*, vol. 7, no. 13, pp. 7436–7444, 2015.

[34] C.-W. Peng, K.-C. Chang, C.-J. Weng et al., "UV-curable nanocasting technique to prepare bio-mimetic superhydrophobic non-fluorinated polymeric surfaces for advanced anticorrosive coatings," *Polymer Chemistry*, vol. 4, no. 4, pp. 926–932, 2013.

[35] H. Chang, K. Tu, X. Wang, and J. Liu, "Facile preparation of stable superhydrophobic coatings on wood surfaces using silica-polymer nanocomposites," *BioResources*, vol. 10, no. 2, pp. 2585–2596, 2015.

[36] I. S. Bayer, "Smart polymer nanocomposite water and oil repellent coatings for aluminum," in *Handbook of Smart Coatings for Materials Protection*, pp. 510–529, Woodhead Publishing, 2014.

[37] S. Nagappan, S. S. Park, and C.-S. Ha, "Recent advances in superhydrophobic nanomaterials and nanoscale systems," *Journal of Nanoscience and Nanotechnology*, vol. 14, no. 2, pp. 1441–1462, 2014.

[38] C. P. Wong, "Recent advances on nanomaterials for advanced packaging applications," in *2012 7th IEEE International Conference on Nano/Micro Engineered and Molecular Systems (NEMS)*, p. 1, IEEE, 2012.

[39] A. Milionis, D. Fragouli, I. Bayer, G. C. Anyfantis, R. Cingolani, and A. Athanassiou, "Magnetically induced drop movement on nano rough micropatterned nanocomposites," in *Technical Proceedings of the 2011 NSTI Nanotechnology Conference and Expo*, vol. 1, pp. 592–595, NSTI-Nanotech, 2011.

[40] Y. Li, R. Zhang, L. Zhu et al., "Nano materials and composites for electronic and photo packaging," in *2009 9th IEEE Conference on Nanotechnology*, pp. 1–3, IEEE NANO, 2009.

[41] C.-H. Chang, M.-H. Hsu, C.-J. Weng et al., "3D-bioprinting approach to fabricate superhydrophobic epoxy/organophilic clay as an advanced anticorrosive coating with the synergistic effect of superhydrophobicity and gas barrier properties," *Journal of Materials Chemistry A*, vol. 1, no. 44, pp. 13869–13877, 2013.

[42] C.-J. Weng, C.-W. Peng, C.-H. Chang, Y.-H. Chang, and J.-M. Yeh, "Corrosion resistance conferred by superhydrophobic fluorinated polyacrylate–silica composite coatings on cold-rolled steel," *Journal of Applied Polymer Science*, vol. 126, no. S2, pp. e48–e55, 2012.

[43] Y. Li, Y. Sun, L. Zhu et al., "Nanocomposite for advanced packaging of microelectronics," in *2006 International Conference on Electronic Materials and Packaging*, pp. 1–16, IEEE, 2006.